# Locating delaminations in laminated composite beams using nonlinear guided waves

Reza Soleimanpour and Ching-Tai Ng*

School of Civil, Environmental & Mining Engineering

The University of Adelaide

Adelaide, SA 5005, Australia

## Abstract

This paper proposes a new method for detecting and locating delaminations in laminated composite beams using nonlinear guided wave. It is shown that when incident wave interacts at the delamination, the nonlinear effect of wave interaction with contact interfaces at the delamination generates higher harmonic guided waves due to contact acoustic nonlinearity (CAN). The proposed method employs a transducer network to detect and locate the delamination using the higher harmonic guided waves. A sequential scan is used to inspect the laminated composite beams by actuating the fundamental anti-symmetric mode ($A_0$) of guided wave at one of the transducers while the rest of the transducers are used for measuring the impinging waves. A series of numerical case studies are performed using three-dimensional explicit finite element simulations, which consider different delamination locations, lengths and through-thickness locations. Experimental case studies are carried out to further validate and demonstrate the capability of the proposed method. The results show that the proposed method is able to accurately detect and locate the delamination in the laminated composite beams using the higher harmonic guided waves. One of the advantages of the proposed method is that it does not rely on baseline data to detect and locate the

* Corresponding author: Dr Ching-Tai Ng, Email: alex.ng@adelaide.edu.au

delamination, and hence, it has less influence by varying operational and environmental conditions.

Keywords: nonlinear guided wave, contact acoustic nonlinearity, higher harmonic, delamination, laminated composite beam, baseline-free method, transducer network

## 1. Introduction

### 1.1. Overview

In last decade, fibre-reinforced composite materials have been widely used in different engineering structures due to its attractive characteristics, such as high specific stiffness, light-weight and corrosion resistance [1]. Delamination is one of the common types of damage for this kind of material and it could lead to structural failure. Delamination is a separation of adjacent subsurface laminae without any obvious visual evidence on the surface and is usually caused by fatigue loading, low velocity impact and imperfection during manufacturing process.

Many techniques have been developed for damage detection in last two decades [2,3]. Low-frequency vibration damage detection approach has been extensively investigated in the literature [4-9]. However, this approach is generally not sensitive to local incipient defects, such as delamination. Non-destructive evaluation techniques [10-15], such as conventional ultrasonic techniques, have been used for safety inspection of a wide range of structures. However, they are a point-to-point inspection method, and hence, the safety inspection is usually time consuming and not applicable to inaccessible locations of structures.

In the recent years, the use of guided waves has attracted considerable attention for damage detection [16-21]. Many studies have been carried out and focused on different types of materials, such as isotropic [22-27] and composite materials [28-30]. In the literature, guided waves have gained prominence for damage detection due to their potential for online

structural health monitoring and inspection at inaccessible locations. Moreover, guided waves have been proved to be sensitive to small and different types of defects and are able to propagate long distance for monitoring relatively large area of structures [16,17]. So far, most of the existing ultrasonic guided wave damage detection techniques rely on linear guided wave scattering phenomena, such as reflection, transmission and mode conversion information at the excitation frequency [31-35]. Majority of these techniques detect the damage by comparing the guided wave signals obtained from the current condition of a structure with signals obtained from its pristine condition. However, the changing environmental and operational conditions, e.g. temperature variation, can significantly affect the performance and accuracy of the damage detection techniques relied on baseline data [36,37] and could lead to misdetection of the damage and false alarms. Therefore, it limits the practical applications of the damage detection techniques using linear guided wave.

### 1.2. Damage detection using nonlinear guided waves

The use of nonlinear guided waves has recently attracted considerable attention. Recent developments have shown that the sensitivity of nonlinear guided waves to small defects is much higher than conventional linear guided waves. Thus, there has been a growing interest in theoretical developments and applied research on using various classical and non-classical nonlinear phenomena for damage detection. The nonlinear guided wave techniques rely on higher harmonic generation due to material nonlinearity [38] or contact acoustic nonlinearity (CAN) [39-43]. The higher harmonic generation has been known to be an indication of defect existence in structures. Early developments on the use of the higher harmonics generated by CAN focused on determining the existence of the defects in the structures. In recent years, significant progress has been made towards using higher harmonic guided waves for damage detection, which demonstrated the feasibility of using them for detecting plastic strain, fatigue damage, micro-cracking and other types of material damages [44-50].

Li et al. [44] proposed to detect thermal fatigue damage in composite laminates using second harmonic Lamb waves. It was shown that there is a monotonic increase of acoustic nonlinearity with respect to thermal fatigue cycles. It was concluded that nonlinear Lamb waves can be used to assess thermal fatigue damage and the technique is better than conventional linear Lamb wave technique in terms of accuracy and efficiency. Soleimanpour and Ng numerically [45] and experimentally [46] investigated the generation of second harmonic when guided waves interact at delamination in laminated composite beams. It was shown that the second harmonics generated due to CAN is sensitive to the existence of delaminations in laminated composite beams. Hong *et al*. [47] investigated the phenomenon of CAN related to breathing fatigue cracks and included material nonlinearity effect in their study. They showed that the relative acoustic nonlinearity parameter increases proportionally with the wave propagation distance due to the geometric and materials nonlinearities. Zhao *et al*. [48] studied the second harmonic generation of Lamb waves in transversely isotropic plate and a symmetric composite laminate. They showed that for transversely isotropic plate, when waves propagate along material principal directions, the symmetric second harmonic Lamb-like waves modes can be generated whereas for propagation direction other than material principal direction only the symmetric second harmonic waves are generated. Moreover, for symmetric composite laminate, only the symmetric second harmonic waves can be generated provided that the power flux is non-zero.

Although extensive research works have been carried out on the use of higher harmonic for damage detection, there were very limited studies [49,50] focused on determining the location of the defects, especially for delamination in laminated composite materials using higher harmonic guided wave generated due to CAN. Kazakov *et al*. [49] proposed a method to determine the location of a crack using high-frequency tone bursts modulated by a continuous low-frequency wave. Experimental verification was carried out using a steel plate. Dziedziech *et al*. [50] proposed a damage detection method based on the

synchronisation of the low-frequency vibration with the interrogating high-frequency guided wave. The method was employed to detect and locate fatigue crack in aluminium beam experimentally. Their results demonstrated the feasibility of using higher harmonic guided wave for baseline-free damage detection.

This paper presents a novel technique for determining the location of delaminations in laminated composite beams using higher harmonic guided wave generated by CAN. The proposed technique has the following advantages: 1) it does not rely on the baseline data for detecting and locating the delaminations, and hence, it has less influence by varying environmental conditions; 2) the nonlinear damage feature is sensitive to small incipient damages.

The paper is organized as follows. Section 2 describes the theoretical background of CAN in generating the higher harmonic guided wave. Section 3 presents the proposed damage detection methodology, which describes the details of the proposed damage detection technique in determining the location of the delamination in laminated composite beams. In Section 4 a series of numerical case studies are presented. In this section, the performance and capability of the proposed damage detection methodology are assessed and demonstrated through a number of numerical case studies. Delaminations with different locations, sizes and through-thickness locations are considered. In Section 5, experimental case studies are presented to verify the applicability of the proposed damage detection method in practical situation. Finally, conclusions are drawn in Section 6.

## 2. Theoretical Background

Higher harmonic generation involves various classical and non-classical nonlinear phenomena in ultrasonic wave responses. Classical nonlinear phenomenon refers to higher harmonic generation due to material imperfections, in which the wave distortion occurs when incident wave interacts with nonlinear elastic response of the medium during the wave

propagation. In the presence of micro-scale damages, e.g. distributed micro-cracks in the materials, the higher harmonic generation is significantly enhanced. The phenomenon of higher harmonic generation due to material nonlinearity was formulated by Hegedron [51], Lee and Choi [52] and Naugolnykhand and Ostrovsky [53]. It was shown that if a harmonic input with a single frequency component of $\omega$ is imposed on a nonlinear system, the output of the system contains higher harmonics of $2\omega$ and $3\omega$. Therefore, the material nonlinearity can be a possible source of the wave nonlinearity.

In non-classical nonlinear phenomenon, higher harmonics can be generated due to CAN, which is a nonlinear effect of wave interaction with contact interfaces at material discontinuities, e.g. fatigue cracks and delaminations. CAN is related to the lack of stiffness symmetry for near-surface strain across the interfaces [40]. Since the compression is accompanied by weakening or rupture of the contact between the surfaces, the compression elasticity is higher than that of a tensile stress. Therefore when the mechanical wave passes through the contact interfaces, a bi-modular area is created and can be simulated by a piece-wise stress–strain relation. This bi-modular surface causes clapping form of behaviour, which is generated due to asymmetry in stress-strain characteristics of damaged interfaces. The formulation of clapping between interfaces was proposed by Solodov *et al*. [40]. Consider a pair of interfaces, subjected to the clapping of the interfaces due to longitudinal or flexural wave. The clapping behaviour, which is caused by asymmetrical dynamics of the interface stiffness, can be approximated by a stress-strain relation as [40]

$$\sigma = E^{II}[1 - H(\varepsilon - \varepsilon^0)\left(\frac{\Delta \mathrm{E}}{E^{II}}\right)]\varepsilon \tag{3}$$

$$\Delta \mathrm{E} = [\mathrm{E}^{II} - \frac{\mathrm{d}\sigma}{d\varepsilon}] \text{ for } \varepsilon>0 \tag{4}$$

where ε is strain and σ is stress, $H(\varepsilon)$ is the Heaviside unit step function and $E^{II}$ is the intact material second-order linear elasticity. $\varepsilon^0$ is the initial static contact strain.

A harmonic strain $\varepsilon(t) = \varepsilon_0 cos\omega t$ of period $T = 2\pi/\omega$, which passes through the bi-modular interface, works like a mechanical diode causing variation in $E^{II}$. In this case the

compressional part of the wave penetrates into the contact region while the tensile part does not. Thus, once the incident wave interacts with the interfaces, the waves shape is rectified nearly half-wave, which provides an unconventional nonlinear waveform distortion as shown in Fig. 1. As $E^{II}$ is a periodic function of the frequency, the induced nonlinear part of spectrum $\sigma^{NL}$ at the damaged area is

$$\sigma^{NL}(t) = \Delta E(t).\varepsilon(t) \tag{5}$$

which consists higher harmonics and the amplitude of the *n*-th harmonic $A_n$ are modulated by the sinc-envelope function as follows [40]

$$A_n = \Delta \mathrm{E}\Delta\tau\varepsilon_0[sinc\big((n+1)\Delta\tau\big) - 2\cos(\pi\Delta\tau)\mathrm{sinc}(\mathrm{n}\Delta\tau) + \mathrm{sinc}((\mathrm{n}-1)\Delta\tau)] \tag{6}$$

$$\Delta\tau = \frac{\tau}{T}, \tau = \frac{T}{\pi}\mathrm{Arc}\cos(\frac{\varepsilon^0}{\varepsilon_0}) \tag{7}$$

where $\Delta\tau$ is the normalized modulation pulse length. When the strain is larger than the threshold of clapping $\varepsilon^0$, i.e. $\varepsilon > \varepsilon^0$, the spectrum of nonlinear vibration contains both odd and even harmonics [40].

*[Fig. 1 CAN strain-stress model and wave rectification]*

## 3. Damage Detection Methodology

The majority of existing damage detection techniques use baseline data for damage detection. It means that damage detection needs to be carried out by comparing the data obtained from the current state of the structure with the baseline data obtained from the pristine structure. However, the varying operational and environmental conditions of the structure can adversely influence the collected data and cause errors [36,37]. To address this problem, this study proposes to use the second harmonic guided wave generated by clapping of delamination interfaces to detect and locate the delaminations in laminated composite beams, and hence, the damage detection does not rely on the baseline data.

It has been shown that the fundamental anti-symmetric mode ($A_0$) of guided wave possesses a smaller wavelength compared to the fundamental symmetric mode ($S_0$) of guided wave at the same frequency. In addition, the anti-symmetric mode guided waves have much larger out-of-plane displacement magnitude than that in in-plane direction. As the out-of-plane displacement is perpendicular to the subsurfaces of the laminae (contact surfaces in CAN) at the delamination, it provides a better correlation in terms of higher harmonic guided wave generation at the delamination. Therefore, $A_0$ guided wave is used as the incident wave in this study.

### 3.1. Transducer arrangement for damage detection

Without loss of generality, a transducer network consists of at least three transducers is used to detect and locate the delamination in the laminated composite beams in this study. Each of the transducers can act as both actuator and receiver for excitation and measurement. The advantage of using the transducer network is that it provides a flexibility of inspecting a long length of one-dimensional (1D) waveguide (e.g. laminated composite beam), which addresses the wave attenuation issue due to material damping of laminated composite materials. In this section a transducer network consists of three transducers, labelled as Transducers 1, 2 and 3, is used to illustrate the concept of the proposed method for detecting and locating the delamination. Fig. 2 shows a schematic diagram of the transducer network arrangement. The laminated composite beam is divided into four zones. A sequential scan for inspecting the laminated composite beam can be performed by actuating the $A_0$ guided wave at one of the transducers while the rest of the transducers are used for measuring the impinging waves.

*[Fig. 2 Schematic diagram of a transducer network for detecting and locating delaminations]*

In general there are two conditions, pulse-echo and pitch-catch, depending on the location of the delamination. Using the transducer network in Fig. 2 as an example, in which Transducers 1 and 2 are used as actuator and receiver, respectively, if the delamination is located in zone 3, it is the pulse-echo condition. Under this condition, Transducer 2 measures the reflected waves, i.e. reflected linear guided wave and higher harmonic guided wave from the delamination. If the delamination is located in zone 2, it is the pitch-catch condition. Transducer 2 measures the transmitted waves, i.e. scattered linear guided wave and higher harmonic guided wave induced at the delamination.

In this study a general approach, which considers both the pulse-echo and pitch-catch condition, is proposed to detect and locate the delamination in the laminated composite beams using the higher harmonic guided wave. Thus the proposed method is applicable to different actuation-sensing situations in the transducer network. Sections 3.2 and 3.3 describe the details of detecting and locating the delamination under the pulse-echo and pitch-catch condition.

### 3.2. Pulse-echo condition

In the case of pulse-echo condition, the delamination is located at one side of both actuator and receiver as shown in Fig. 3c. The incident wave generated by the actuator passes through the receiver and then reaches the delamination. The receiver measures the reflected linear guided wave and the second harmonic guided wave induced due to the interaction of the incident wave with the delamination. The linear guided wave reflection is at the same frequency as the incident wave ($f_c$) while the second harmonic guided wave is at frequency $2f_c$.

Figs. 3a and 3b show a schematic diagram of the incident wave and the second harmonic guided wave in time-domain and time-frequency domain, respectively. The incident wave and second harmonic guided wave package arrive the receiver at different

times, i.e. $t_{f_c}$ and $t_{2f_c}$. As shown in time-frequency energy density spectrum in Fig. 3b, there are three contours. Two contours are at the excitation frequency $f_c$ and the other contour is at frequency $2f_c$. The two contours at $f_c$ refer to the incident wave and reflected linear guided wave package from the delamination while the contour at frequency $2f_c$ refers to the second harmonic guided wave package generated due to CAN at the delamination.

The arrival time of the incident wave ($t_{f_c}$) is

$$t_{f_c} = \frac{d_{a-r}}{c_g(f_c)} \tag{14}$$

where $d_{a-r}$ is the distance between the actuator and receiver as shown in Fig. 3c and $c_g(f_c)$ is the group velocity of the incident $A_0$ guided wave at the excitation frequency $f_c$. The arrival time of the second harmonic guided wave package ($t_{2f_c}$) is

$$t_{2f_c} = \frac{d_{a-r}}{c_g(f_c)} + \frac{d_{d-r}}{c_g(f_c)} + \frac{d_{d-r}}{c_g(2f_c)} \tag{15}$$

where $c_g(2f_c)$ is the group velocity of the second harmonic guided wave and $d_{d-r}$ is the distance between the delamination and the receiver. Therefore, using Equations (14) and (15), the delamination location can be determined by

$$d_{d-r} = \frac{\Delta t . c_g(2f_c) . c_g(f_c)}{c_g(2f_c) + c_g(f_c)} \text{ where } \Delta t = t_{2f_c} - t_{f_c} \tag{16}$$

where $\Delta t$ is the time difference between the arrival time of the incident wave ($t_{f_c}$) and the second harmonic guided wave ($t_{2f_c}$). Once the value of $\Delta t$ is determined from the measured guided wave data, the delamination location $d_{d-r}$ can be obtained.

In the case of using linear guided wave information to detect and locate the delamination, it usually requires the baseline data to extract the linear scattered wave information when the delamination is close to the receiver or the beam is relatively short as the linear scattered wave overlaps with the incident wave or wave reflected from boundaries. In contrast the determination of the delamination location $d_{d-r}$ using the higher harmonic guided wave, it only relies on the information of $t_{f_c}$ and $t_{2f_c}$, i.e. the arrival time of the

incident wave and second harmonic guided wave, as shown in Equation (16). Thus the delamination can be detected and located without the baseline data.

*[Fig. 3 Typical signal in time domain, time-frequency domain and schematic diagram of the (a)-(c) pulse-echo and (d)-(f) pitch-catch condition]*

### 3.3. Pitch-catch condition

For the pitch-catch condition, the delamination is located between actuator and receiver as shown in Fig. 3f. Different to pulse-echo condition, the incident wave generated by the actuator first interacts with the delamination and then reaches the receiver. When the incident wave interacts with the delamination, it induces a linear scattered wave and a second harmonic guided wave due to CAN at the delamination. Figs. 3d and 3e show a schematic diagram of the incident wave and the second harmonic guided wave in time-domain and time-frequency domain, respectively. As shown in Fig. 3d the transmitted wave package contains the incident wave, linear scattered wave and second harmonic guided wave. The arrival time of the incident wave and higher harmonic guided wave are $t_{f_c}$ and $t_{2f_c}$, and they can be obtained at frequencies $f_c$ and $2f_c$ in the time-frequency domain, respectively.

The arrival time of the incident wave travel from the actuator to the delamination and then to the receiver ($t_{f_c}$) is

$$t_{f_c} = \frac{d_{a-d} + d_{d-r}}{c_g(f_c)} \tag{17}$$

where $d_{a-d}$ is the distance between the actuator and delamination in the pitch-catch condition. The arrival time of the second harmonic guided wave is

$$t_{2f_c} = \frac{d_{a-d}}{c_g(f_c)} + \frac{d_{d-r}}{c_g(2f_c)} \tag{18}$$

Using Equations (17) and (18), the delamination location $d_{r-d}$ can be determined by

$$d_{d-r} = \frac{\Delta t.c_g(2f_c).c_g(f_c)}{-c_g(2f_c)+c_g(f_c)} \text{ where } \Delta t = t_{2f_c} - t_{f_c} \tag{19}$$

Under the pitch-catch condition, if the excitation frequency is at the flat region of the $A_0$ group velocity dispersion curve, the group velocity of the higher harmonic guided wave $c_g(2f_c)$ is almost the same as the group velocity of the linear incident wave $c_g(f_c)$, and hence, $\Delta t \approx 0$. In this case, although information is not enough to determine the delamination location $d_{d-r}$ in the pitch-catch approach, it can still indicate the existence of the delamination and also the delamination zone based on the presence of higher harmonic guided wave measured by the actuator-receiver pair. If the excitation frequency is at the dispersive region of the $A_0$ group velocity dispersion curve, i.e. the low frequency non-flat region, the group velocity of the higher harmonic guided wave $c_g(2f_c)$ is different to the incident wave $c_g(f_c)$. In this case, $\Delta t \neq 0$, and hence, the delamination location $d_{d-r}$ can be determined without the baseline data. In contrast, the pitch-catch approach using the linear guided wave does not provide enough information to determine the delamination location even the baseline data is available. Therefore, the use of the higher harmonic guided wave can provide additional information in damage detection.

### 3.4. Determination of delamination zone and location

In this study, the excitation frequency is selected at the flat region of the $A_0$ group velocity dispersion curve, and hence, it can minimise the dispersion effect of the $A_0$ guided wave to maximize the wave propagation distance. Under this situation, the group velocity of the higher harmonic guided wave is almost the same as the linear incident wave, therefore, the pitch-catch condition is only used to determine the existence of the delamination and the delamination zone.

In practical situation, the existence and location of the delamination are unknown before the damage detection. A sequential scan is required to detect and locate the delamination using the transducer network as shown in Fig. 2, and hence, the actuator-receiver pair can be under pulse-echo or pitch-catch condition depending the location of the

delamination. As discussed in Sections 3.2 and 3.3, if the difference of the arrival time between the incident wave and higher harmonic guided wave obtained from the measured data is $\Delta t \approx 0$, i.e. $d_{d-r} \approx 0$, this means it is the pitch-catch condition, and hence, the delamination is located within this actuator-receiver pair. Therefore, the delamination zone can be identified. The location of the delamination can be determined by using the other actuator-receiver pair under the pulse-echo condition. In this case $\Delta t$ can be obtained from the measured data to determine the delamination location based on the Equation (16).

Table. 1 summarises all possible combinations in estimating the delamination location using a sequential scan of the transducer network with three transducers. The delamination location determined using the data measured by Transducer *i* is defined as $d_{d-i}$ in Table 1. $d_{d-i}$ is the distance of the delamination away from the Transducer *i*. Using Transducer 1 as the actuator, the rest of the transducers as receivers, and the delamination is located in zone 2 as an example, $d_{d-2} \approx 0$ and $d_{d-3} \approx 0$. It then needs to consider using Transducer 2 as the actuator. In this case, $d_{d-1} \approx 0$ and $d_{d-3} > 0$. Therefore the delamination is in zone 2 and the location is $d_{d-3}$. Similarly the delamination location can be obtained by using Transducer 3 as the actuator for the delamination located in zone 2, in which $d_{d-1} \approx 0$ but $d_{d-2} > 0$. This means the delamination is in zone 2 and the location is $d_{d-2}$. In general, damage zone can be identified using any actuator-receiver under the pitch-catch condition and at least an actuator-receiver pair needs to be under pulse-echo condition for determining the delamination location. Since the delamination location is calculated based on the information of the incident wave and second harmonic guided wave, it can be detected and located without using the baseline data.

*[Table 1. Possible combinations for estimating the delamination location using a sequential scan of a transducer network with three transducers for delamination located at different zones]*

### 3.5. Continuous Gabor wavelet transform

In this study the measured data is processed by the continuous Gabor wavelet transform, and hence, the time-frequency energy density spectrum can be obtained to accurately estimate the arrival time of the incident wave and the higher harmonic guided wave from the delamination. The continuous wavelet transform (CWT) displays the scale-dependent structure of a signal as it varies in time. This scale-dependent structure is essentially the frequency. Therefore, CWT provides a view of the frequency versus time behaviour of the signal [54]. The wavelet coefficient $WT(p,q)$ can be obtained by convolving the measured guided wave signal $u(t)$ with the translation $p$ and dilation $q$ as

$$WT(p,q) = \int_{-\infty}^{\infty} u(t)\chi_{p,q}^{*}(t)dt \tag{21}$$

where

$$\chi_{p,q}(t) = \frac{1}{\sqrt{q}}\chi\left(\frac{t-p}{q}\right) \tag{22}$$

The asterisk donates the complex conjugate. $\chi(t)$ is the mother wavelet and Gabor wavelet is used in this study. The Gabor wavelet is defined as

$$\chi(t) = \frac{1}{\sqrt[4]{\pi}}\sqrt{\frac{\omega_0}{\eta}}\exp\left[-\frac{(\omega_0/\eta)^2}{2}t^2 + i\omega_0 t\right] \tag{23}$$

The time-frequency analysis resolution depends on the value of $\omega_0$ and $\eta$. These values are usually considered as $\omega_0 = 2\pi$ and $\eta = \pi\sqrt{2/\ln 2} \approx 5.336$. The energy density spectrum is calculated by $|WT(p,q)|^2$, which indicates the energy distribution of the signal around $t = p$ and $\omega = \omega_0/q$. Thus, the energy density spectrum can be used to calculate the arrival time of the incident wave and higher harmonic guided wave at a specific frequency, and hence, the delamination location can be accurately identified.

## 4. Numerical Case Studies

An eight-ply $[(0/90)_2]_S$ laminated composite beam with a delamination was considered in this study. The dimensions of the beam is 166 mm × 12 mm × 1.6 mm. The elastic properties of

the lamina are shown in Table. 2, and the thickness and density are 0.2 mm and 1538 kg/m$^3$, respectively. The delaminations considered in the numerical case studies have different locations, sizes and through-thickness locations. In this study a three-dimensional (3D) explicit finite element method [55] was used to simulate the propagation of linear and higher harmonic guided wave in the laminated composite beam. The model was created in ABAQUS®/CAE and the simulations were solved by the explicit finite element code in ABAQUS/Explicit, which uses the central-difference integration [55]. In this scheme, the integration operator matrix is inverted and a set of nonlinear equilibrium equations is solved at each time increment. The increment time step is automatically calculated by ABAQUS.

*[Table 2. Elastic properties of the lamina]*

Each lamina was modelled using a layer of eight-noded 3D full integration linear solid elements (C3D8I) with incompatible mode and hourglass control. The incompatible mode elements have more internal degrees-of-freedom (DoFs) compared to reduced integration mode elements. Each node of the solid brick element has three translational DoFs. The hourglass energy was limited to less than 2% of the total energy to ensure the accuracy of the finite element simulations [56]. Damping effect of the composite materials was considered in the simulation. It was simulated using the Rayleigh mass proportional and stiffness proportional damping using experimentally obtained results from the specimens with the same material properties in the Section 5. The $A_0$ guided wave was used as the incident wave and it was simulated by applying out-of-plane nodal displacements to surface nodes of the beam, which simulates a piston type excitation generated by a 12 mm × 6 mm rectangular transducer. The in-plane dimensions of the elements were 0.4 mm × 0.4 mm and the thickness was 0.2 mm for all finite element models. The delamination was modeled by duplicating the finite element nodes at the delamination region, which allows two sub-laminate interfaces located at the delamination region move independently. Contact-pair

interaction with associated properties was assigned to the sub-laminate interfaces at the delamination to model the CAN effect described in Section 2. It should be noted that in real situation, the delamination interfaces include some closing stresses due to fibre or matrix bridging. In the numerical case studies, the pure clapping effect was considered at the delaminations, which means no static contact strain is considered in the finite element simulations. However, the experimental study in Section 5 will provide a more realistic situation for verifying the proposed damage detection technique.

In the numerical case studies the excitation signal was a 70 kHz narrow-band five-cycle sinusoidal tone burst modulated by a Hanning window. The wavelength of the $A_0$ guided wave at this excitation frequency and second harmonic frequency are 16 mm and 8 mm, respectively. The group velocity of the guided wave was calculated using the CWT described in Section 3.5 and compared with experimentally measured results. Fig. 4 shows the group velocity dispersion curve of the $A_0$ guided wave. There is a good agreement between the results of the numerical simulations and experimental data. The noise effect was considered in the numerical data, which was simulated by adding white noise to the time-domain guided wave response. The noise level considered in this study was approximately 1% of the maximum amplitude of each signal, which is similar to the noise level observed in the experimental data in Section 5.

*[Fig 4. Group velocity dispersion curves of $A_0$ mode guided wave]*

Using the transducer network as shown in Fig. 2, two scenarios are considered in this study. Scenario 1 considers the delamination located in zone 3, i.e. between Transducers 2 and 3, while Scenario 2 considers the delamination located in zone 4, i.e. at the beam end. Each scenario was studied numerically in this section and also experimentally in Section 5. The distance between each transducer is 50 mm and the Transducers 1 and 3 are located at 33 mm away from the left and right beam ends, respectively. Different delamination lengths

from 4 mm to 16 mm in steps of 4 mm were considered in the numerical case studies. Without loss of generality, the delamination lengths are presented in term of the delamination length to the wavelength of the incident linear $A_0$ guided wave ratio $d/\lambda$. Figs. 5a and 5b show the details of the Scenarios 1 and 2 with delamination length of 8 mm, i.e. $d/\lambda = 0.5$. For each delamination length, different delamination through-thickness locations were considered, i.e. the delaminations were located between the first and second, the second and third and third and fourth layers of the laminated composite beams. Table 3 shows a summary of damage cases considered in each scenario. In each scenario, 12 damage cases considering different lengths of delaminations located at different through-thickness locations were used to verify and demonstrate the performance of the proposed method in detecting and locating the delaminations. In total there were 24 damage cases considered in the numerical case studies.

*[Fig. 5 a) Schematic diagram of Scenario 1 and b) 2 in numerical case studies]*

*[Table 3. Summary of delamination sizes and through-thickness locations of damage cases for each scenario in numerical studies]*

### 4.1. Scenario 1: Delamination is located between the actuator-receiver pair

Fig. 6 shows a snapshot of the finite element simulation results when the $A_0$ guided wave interacting with the delamination located at third and fourth layers in the laminated composite beam (Damage Case $B_3$), in which $d/\lambda = 0.5$. As shown in Fig. 6, the contact interaction applied to the subsurfaces of the laminae at the delamination, which prevents the interpenetration between the subsurfaces and simulates the CAN in delamination area.

*[Fig. 6. A snapshot of the $A_0$ guided wave interacting with the delamination in Damage Case $B_3$]*

The data simulated was the time-domain out-of-plane displacement responses at the location of the transducers. Figs. 7a-7c show the acquired data at the measurement locations in time-domain when the incident wave was excited at Transducer 1 and the data was measured at Transducer 2. In addition to the calculated time-domain data, the data proceed with Fast Fourier transform (FFT) is also shown in Fig. 7. According to the arrival time of the wave packages in Fig. 7, the first, second and third wave packages attribute to the incident wave, linear reflected wave from the delamination and wave reflection from the beam end, respectively. As the linear reflected wave from the delamination is slightly overlapped with the incident wave package, it is difficult to accurately determine the arrival time of the linear reflected wave without the baseline data, especially for more complicated structures or delamination is close to the receivers. As shown by the frequency-domain data in Fig. 7, second harmonic was observed in all damage cases. To ensure the second harmonic was generated by the CAN at the delamination, an intact laminated composite beam was also created using the finite element method. It was confirmed that there is no higher harmonic in the intact laminated composite beam.

*[Fig 7. Simulated signal in time-domain and frequency-domain for Damage Cases a) $B_1$ b) $B_2$ and 3) $B_3$ in numerical case studies]*

Although the presence of higher harmonic components in frequency-domain can indicate the existence of the delamination in the laminated composite beam, more information is required, i.e. arrival time of the second harmonic guided wave, to locate the delamination. Therefore, the simulated data was transformed to time-frequency domain using CWT described in Section 3.5. Figs 8a, 8b, 8d, 8e, 8g, and 8h show the time-frequency energy density spectrum, which are zoomed-in at frequency ranges around the excitation and second harmonic frequency for Damage Cases B1 and B2 and B3. The information is useful for determining the location of the delaminations. As shown in the time-frequency energy

density spectrum, the energy is concentrated at two frequencies, i.e. around the excitation frequency and second harmonic frequency. Figs. 8c, 8f and 8i also show the corresponding normalized wavelet coefficients at the excitation frequency and second harmonic frequency. The arrival time of the incident wave and second harmonic guided wave, which were determined based on the maximum magnitude of the normalized wavelet coefficients at the excitation frequency and second harmonic frequency, respectively, are indicated by vertical dash-dotted lines. The estimated $\Delta t$ are also indicated in the figures. As shown in Figs. 8c, 8f and 8i, at double frequency, several smaller humps can be observed before the arrival time of second harmonic wave. They may be higher harmonic waves induced due to mode conversion effect, i.e. in-plane waves, when the incident $A_0$ wave interacting at the delaminations not located at the mid-plane of the laminated composite beams. However, these in-plane waves usually have smaller magnitude than the flexural higher harmonic waves in both numerical and experimental case studies.

*[Fig. 8. Time-frequency energy density spectrum, and corresponding normalised wavelet coefficient at excitation frequency (solid line) and second harmonic frequency (dashed line) for Damage Cases (a)-(c) $B_1$, (d)-(f) $B_2$ and (g)-(i) $B_3$ (vertical dash-dotted lines: estimated arrival times)]*

For Damage Case B1, the arrival time of the incident wave and second harmonic guided wave at the excitation frequency and second harmonic frequency are 66.0 μsec and 100.3 μsec, respectively. Hence, the estimated delamination location from the receiver using Equation (16) is $d_{d-2}$ = 23.9 mm from the Transducer 2 (delamination located between Transducers 2 and 3). Similarly, the estimated delamination location from the receiver for Damage Cases B2 and B3 are $d_{d-2}$ = 25.9 mm and $d_{d-2}$ = 23.5 mm, respectively. It should be noted that the true left and right end location of the delamination are at 21 mm and 29 mm from the receiver (Transducer 2), i.e. $\bar{d}_{d-2} = 21\,mm - 29\,mm$. Since the higher harmonic guided wave is contributed by the occurrence of CAN at different locations within the

delamination region, i.e. 21 mm – 29 mm, the identified delamination location within this range is considered to be reasonably accurate. The results of other damage cases are summarised in Table 4. In Scenario 1, the delamination is located in zone 3, the delamination distance from Transducer 2 ($d_{d-2}$) is useful for estimating the delamination location as the actuator-receiver pair (Transducer 1 – Transducer 2) is under the pulse-echo condition. Therefore, the results of $d_{d-2}$ are included in Table 4. The results confirm that the proposed technique can detect and locate the delaminations without using the baseline data. As shown in Table 4, the delamination locations are accurately estimated in all damage cases.

*[Table 4. Summary of the results for all damage cases in the numerical case studies]*

### 4.2. Scenario 2: Delamination is located at the beam end

Scenario 2 considers the delamination located at the beam end. The time-domain signal measured by Transducer 3 while the Transducer 2 is used as actuator shows that the signal is more complicated compared to the signal in Scenario 1. Fig. 9a shows the reflected wave from the delamination is hidden in incident wave reflected from the beam end in Damage Case C2. It is impossible to extract the information of the reflected linear wave from the delamination without the baseline data. However, the second harmonic can still be observed in the frequency-domain as shown in Fig. 9b, which indicates the existence of the delamination. With the simulated signals from other actuator-receiver pairs, the delamination zone can be identified if the determined delamination location is close to zero. After that, the signal simulated by the actuator-receiver pair under the pulse-echo condition is used to estimate the delamination location. Table 5 summarises the estimated delamination locations for all damage cases and the results show that the delamination locations are accurately determined using the second harmonic guided wave without the baseline data.

*[Fig. 9 Simulated signal in time-domain and frequency-domain for Damage Case $C_2$ in numerical case studies]*

*[Table 5. Summary of all results for Scenario 2 in the numerical case studies]*

## 5. Experimental Case Studies

In experimental case studies, two eight-ply $[(0/90)_2]_S$ laminated composite beams were manufactured. The specimens were made by unidirectional carbon/epoxy prepreg. The elastic properties of the lamina are $E_{11}$ = 120.20 GPa, $E_{22}$ = $E_{33}$ = 7.47 GPa, $G_{11}$= $G_{12}$ = 3.94 GPa, $G_{13}$ = 2.31 GPa, $\nu_{12}$ = 0.32, $\nu_{23}$ = $\nu_{13}$= 0.33 and $\nu_{13}$ = 0.32, which are the same as the material properties used in the finite element model as shown in Table 2. The lamina has a fibre volume fraction of 0.55, with density and thickness being 1538 kg/m$^3$ and 0.2 mm, respectively.

The dimensions of the laminated composite beams are 166 mm × 12 mm × 1.6 mm, which are the same as the numerical case studies. There is a 15 mm long delamination in each composite beam specimen. In Damage Case 1, the delamination is located between the third and fourth ply. The true right and left end locations of the delamination are at 17.5 mm and 32.5 mm, respectively, i.e. $\bar{d}_{d-2}$ = 17.5 mm – 32.5 mm at the right hand side of the Transducer 2. In Damage Case 2, the delamination is located between the third and fourth ply and between the Transducer 3 and the right beam end. The true left and right end locations of the delamination are at 18 mm and 33 mm from the Transducer 3, i.e. ($\bar{d}_{d-3} = 18\,mm - 33\,mm$). The details of the laminated composite beam specimens and the location of the transducers are shown in Fig 10. The delamination in the laminated composite beam specimen was created by inserting two very short Teflon films at the required through-thickness location during the manufacturing process. A three-point bending test was then employed to grow the delamination to the required length by breaking the weak bonding

between the plies and Teflon film. Therefore, there is still a certain level of the static contact strain effect considered in the experimental study.

*[Fig. 10 Schematic diagram of composite beam specimens with a delaminations for a) Damage Case 1 b), Damage Case 2 and c) cross-section at delamination location in experimental case studies]*

A computer controlled National Instrument PXIe-1073 chassis, which consists of a NI PXI-5412 arbitrary waveform generator and a NI PXI-5105 digitizer was used in the experimental study. Three rectangular piezoceramic transducers with dimension 12 mm × 6 mm × 2 mm were adhesively bonded to the surface of each of the laminated composite beam specimen. The excitation signal was generated by the arbitrary waveform generator and then amplified by an amplifier with peak-to-peak voltage of 50 V. The responses of the receiver were recorded by digitizer and then sent to the computer. Fig. 11 shows the schematic diagram of the experimental setup. The excitation signal is the same as the numerical case studies in Section 4, i.e. a 70kHz narrow-band five-cycle sinusoidal tone burst modulated by a Hanning window. Prior to each measurement, it was confirmed that there was no inherent nonlinearity induced by the electrical equipment at the selected excitation frequency. Moreover, to further ensure that the captured higher harmonics are not generated due to the inherent nonlinearity of electrical equipment or the debonding of piezoelectric transducers, an intact laminated composite beam specimen was used to confirm there is no non-damage related higher harmonic induced in the experiments.

*[Fig. 11 Experimental setup]*

The transducers were actuated sequentially, in which one of the transducers was used to generate the incident wave while the other two transducers were used for data acquisition. The delamination zone was first identified using Table 1. Figs. 12a and 12b show the

measured results by one of the actuator-receiver pairs in the frequency-domain. Fig. 12a is the data measured by Transducer 2 while Transducer 3 was used as the actuator in Damage Case 1. In Fig. 12b, the data was measured using Transducer 3 while Transducer 2 was the actuator in Damage Case 2. As shown in Fig.12a and 12b, the higher harmonics induced due to the clapping effect at the delamination interfaces are observed in both damage cases.

*[Fig. 12. Measured signal in frequency-domain, a) Transducer 2 is the receiver while Transducer 3 is the actuator in Damage Case 1, b) Transducer 3 is the receiver while Transducer 2 is the actuator in Damage Case 2]*

To determine the delamination location, the measured data was transformed to time-frequency domain using CWT. Fig. 13a and 13b show the time-frequency energy density spectrum for Damage Cases 1 and 2, respectively. The normalized CWT coefficient at the incident wave frequency and second harmonic frequency are also shown in Figs. 13c and 13f. In Damage Case 1, the arrival time of the incident wave and second harmonic guided wave are 69.8 μsec and 116.4 μsec, respectively. The estimated delamination location is $d_{d-2}$ = 32.5 mm from the receiver (Transducer 2), which is within the true delamination location range, i.e. $\bar{d}_{d-2}$ = 17.5 mm – 32.5mm. In Damage Case 2, the arrival time of the incident wave and second harmonic guided wave are 79.8 μsec and 107.9 μsec, respectively. Therefore the estimated delamination location is $d_{d-3}$ 19.6 mm, which is again within the true delamination location range, i.e. $\bar{d}_{d-3}$= 18 mm – 33 mm. Overall the results show that the delamination location can be accurately determined without using the baseline data.

*[Fig 13. Time-frequency energy density spectrum zoom-in, and the corresponding normalised CWT coefficients at excitation frequency (solid line) and second harmonic frequency (dashed line) for a) Damage Case 1 and b) Damage Case 2 (vertical dash-dotted lines: estimated arrival times)]*

## 6. Conclusions

In this study, a baseline-free method has been proposed to detect and locate the delaminations in laminated composite beams using the generated higher harmonic guided wave due to clapping effect, i.e. CAN, at delaminations. To take into account the practical situation, the proposed method employs a transducer network consisting at least three transducers. A sequential scan for inspecting the laminated composite beam has been performed by actuating $A_0$ guided wave at one of the transducers while the rest of the transducers are used for measuring the impinging waves. The proposed method covers all possible conditions, i.e. both pulse-echo and pitch-catch condition, in using the higher harmonic guided wave and the transducer network to detect and locate the delamination without the baseline data. The continuous Gabor wavelet transform has been used to extract the arrival time information of the higher harmonic guided wave. A series of numerical case studies have been carried out, which have considered 24 damage cases with different delamination locations, lengths and through-thickness locations. Experimental case studies have also been carried out to further validate and demonstrate the capability of the proposed method. Overall the results show that the proposed method is able to accurately detect and locate the delamination in the laminated composite beams without using the baseline data. Although this study focuses on laminated composite beams, the proposed method is general and can be applied to metallic material in different engineering structures, e.g. civil, aerospace and mechanical engineering. It should be noted that further studies are required to investigate the feasibility of extending the proposed method for damage quantification.

## 7. **Acknowledgement**

This work was supported by the Australian Research Council under Grant Number DP160102233.

## 8. References


1. Wang K, Young B, Smith ST. Mechanical properties of pultruded carbon fibre-reinforced polymer (CFRP) plates at elevated temperatures. Eng Struct, 2011; 33: 2154-2161.
2. Kim JT, Ryu YS, Cho HM, Stubbs N. Damage identification in beam-type structures: frequency-based method vs mode-shape-based method. Eng Struct, 2003; 25: 57–67.
3. Yin T, Lam HF, Chow HM, and Zhu HP. Dynamic Reduction-Based Structural Damage Detection of Transmission Tower Utilizing Ambient Vibration Data. Eng Struct, 2009; 31(9): 2009-2019.
4. Salawu OS. Detection of structural damage through changes in frequency: a review. Eng Struct 1997; 19(8): 718-723.
5. Lam HF and Yin T. Statistical Detection of Multiple Cracks on Thin Plates Utilizing Dynamic Response, Eng Struct 2010: 32(10): 3145-3152.
6. Kim JT, Ryu YS, Cho HM, Stubbs N. Damage identification in beam-type structures: Frequency-based method vs mode-shape-based method. Eng Struct 2003; 25:57-67.
7. Sahin M, Shenoi RA. Quantification and localisation of damage in beam-like structures by using artificial neural networks with experimental validation. Eng Struct 2003; 25:1785-1802.
8. Chow HM, Lam HF, Yin T and Au SK. Optimal Sensor Configuration of a Typical Transmission Tower for the Purpose of Structural Model Updating. Struct Contol Health Monitor 2011: 18(3): 305–320.
9. Sohn H, Farrar CR, Hemez FM, Shunk DD, Stinemates DW, Nadler BR. A review of structural health monitoring literature from 1996–2001. Los Alamos National Laboratory, Los Alamos, NM, report no LA-13976-MS; 2004.
10. Hu H, Wang J. Damage detection of a woven fabric composite laminate using a modal strain energy method. Eng Struct 2009; 31: 1042-1055.
11. Selva P, Cherrier O, Budinger V, Lachaud F, Morlier J. Smart monitoring of aeronautical composites plates based on electromechanical impedance measurements and artificial neural networks. Eng Struct 2013; 56: 794-804.
12. Martin J, Hardy M.S.A., Usmani A.S., Forde M.C. Accuracy of NDE in bridge assessment. Eng Struct 1998; 20: 979-984.
13. Orban Z, Gutermann M. Assessment of masonry arch railway bridges using non-destructive in-situ testing methods. Eng Struct 2009; 31: 2287-2298.
14. Santos P., Julio E, Santos J. Towards the development of an in situ non-destructive method to control the quality of concrete-to-concrete interfaces 2010 Eng Struct; 32: 207-217.
15. Ramos L.F., Miranda T., Mishra M., Fernandes F.M., Manning E. A Bayesian approach for NDT data fusion: the Saint Torcato church case study 2015 Eng Struct; 84: 120-129.

16. Cawley P, Alleyne D. The use of Lamb wave for the long range inspection of large structure. Ultrasonics 1996; 34: 287-290.
17. Rose JL. A baseline and vision of ultrasonic guided wave inspection potential. J Press Vessel Tech 2002; 124: 273-282.
18. Ng CT. On the selection of advanced signal processing techniques for guided wave damage identification using a statistical approach. Eng Struct 2014; 67: 50-60.
19. Ng CT. Bayesian model updating approach for experimental identification of damage in beams using guided waves. Struct Health Monitor 2014; 13: 359-373.
20. Mitra M, Gopalakrishnan S. Guided wave based structural health monitoring: A review. Smart Mater Struct 2016; 25: 053001.
21. He S, Ng CT. A probabilistic approach for quantitative identification of multiple delaminations in laminated composite beams using guided waves. Eng Struct 2016; 127: 602-614.
22. Giurgiutiu V, Bao JJ. Embedded-utlrasonics structural radar for in situ structural health monitoring of thin-wall structures. Struct Health Monitor 2004; 3: 121-140.
23. Ihn JB, Chang FK. Pitch-catch active sensing methods in structural health monitoring for aircraft structures. Struct Health Monitor 2008;7: 5-15.
24. Ng CT. A two-stage approach for quantitative damage imaging in metallic plates using Lamb wave. Earthquake Struct 2015; 8:f 821-841.
25. Haynes C, Todd M. Enhanced damage localization for complex structures through statistical modelling and sensor fusion. Mech Syst Sig Process 2015; 54-55: 195-209.
26. Soleimanpour R, Ng CT. Scattering of the fundamental anti-symmetric Lamb wave at through-thickness notches in isotropic plates. J Civil Struct Health Monitor 2016; 6: 1-13.
27. He S, Ng CT. Guided wave-based identification of multiple cracks in beams using a Bayesian approach. Mech Syst Sig Process 2017; 84: 324-345.
28. Sohn H, Park G, Wait JR, Limback NP, Farra CR. Wavelet-based active sensing for delamination detection in composite structures. Smart Mater Struct 2004; 13:153-160.
29. Ostachowicz W, Kudela P, Malinowski P, Wandowski T. Damage localisation in plate-like structures based on PZT sensors. Mec Syst Sig Process 2009; 23: 1805-1829.
30. Soleimanpour R, Ng CT. Mode conversion and scattering analysis of guided waves at delaminations in laminated composite beams. Struct Monitor Maintenance 2015; 2: 213-236.
31. Rajagopal P, Lowe, MJS. Scattering of the fundamental shear horizontal guided wave by a part-thickness crack in an isotropic plate. J Acoust Soc Am 2008, 124: 2895-2904.
32. Yeum CM, Sohn H, Lim HJ, Ihn JB. Reference-free delamination detection using Lamb waves. Struct Con Health Monitor 2013; 21: 675-684.
33. He S, Ng CT. Analysis of mode conversion and scattering of guided waves at cracks in isotropic beams using a time-domain spectral finite element method. Elec J Struct Eng 2015; 14: 20-32.

34. Ramdhas A, Pattanayak RK, Balasubramaniam K, Rajagopal P. Symmetric low-frequency feature-guided ultrasonic waves in thin plates with transverse bends. Ultrasonic 2015; 56: 232-242.
35. Ng CT. On accuracy of analytical modelling of Lamb wave scattering at delaminations in multilayered isotropic plates. Inter J Stuct Stab Dyn 2015, 15: 1540010.
36. Konstantinidis G, Drinkwater BW, and Wilcox PD. The temperature stability of guided wave structural health monitoring systems. Smart Mater. Struct 2006;. 15: 967–976.
37. Aryan P, Kotousov A, Ng CT and Wildy S. Reconstruction of baseline time-trace under changing environmental and operational conditions. Smart Mater Struct 2016; 25: 035018.
38. Bermes C, Kim JY, Qu J, Jacobs LJ. Nonlinear Lamb waves for the detection of material nonlinearity. Mech Sys Sig Process 2008; 22: 638-646.
39. Donskoy D, Sutin A, Ekimov A. Nonlinear acoustic interaction on contact interfaces and its use for non-destructive testing. NDT & E Inter 2001; 34: 231-238.
40. Solodv IY, Krohn N, Busse G. CAN: An example of nonclassical acoustic nonlinearity in solids. Ultrasonics 2002; 40: 621-625.
41. Klepka A, Staszewski W, Jenal RB, Szwedo M, Iwaniec J, Uhl T. Nonlinear acoustics for fatigue crack detection – experimental investigations of vibro-acoustic wave modulations. Struct Health Monitor 2012; 11: 197-211.
42. Blanloeuil P, Croxford A.J and Meziane A, Application of the noncollinear mixing method to an interface of contact. AIP Conf. Proc. 2012; 1581, 623.
43. Blanloeuil P, Meziane A, Bacon C, Numerical study of nonlinear interaction between a crack and elastic waves under an oblique incidence. Wave Motion 2014; 51(3):425-437.
44. Li W, Cho, Y, Achenbach JD. Detection of thermal fatigue in composites by second harmonic Lamb waves. Smart Mater Struct 2012; 21: 085019.
45. Soleimanpour R, Ng CT. Numerical study of nonlinear guided waves in laminated composite beams with delaminations. 8th Australasian Congress on Applied Mechanics: ACAM8. Barton, ACT, Engineers Australia, 2014: 379-388.
46. Soleimanpour R, Ng CT. Higher harmonic generation of guided waves at delaminations in laminated composite beams. Struct Health Monitor 2016, doi:10.1177/1475921716673021 (online first).
47. Hong M, Su Z, Wang Q, Cheng L and Qing X. Modelling nonlinearities of ultrasonic waves for fatigue damage characterization. Ultrasonics 2014; 54: 770-778.
48. Zhao J, Chillara VK, Ren B, Cho H, Qiu J, Lissenden, CJ. Second harmonic generation in composites: Theoretical and numerical analyses. J Applied Phy 2016; 119: 064902.
49. Kazakov VV, Sutin A, Johnson PA. Sensitive imaging of an elastic nonlinear wave-scattering source in a solid. Applied Phy Letters 2002; 81: 646-648.

50. Dziedziech K, Pieczonka L, Kijanka P, Staszewski W. Enhanced nonlinear crack-wave interactions for structural damage detection based on guided ultrasonic waves. Struct Control Health Monitor 2016, 23: 1108-1120.
51. Hagedorn, P, Schramm, W. On the dynamics of large systems with localized nonlinearities. J Applied Mech, ASME 1988 55:946-951.
52. Lee LH, Choi IH, Jhang KY. The nonlinearity of guided wave in an elastic plate. Mod Phys Letter 2008; 22: 1135-1140.
53. Naugolnykh K, Ostrovsky L. Nonlinear Wave Processes in Acoustics. Cambridge University Press 1998.
54. Ng CT, Veidt M, Rajic N. Integrated piezoceramic transducers for imaging damage in composite lamiantes. Proc SPIE7493 2009; 7493M.
55. ABAQUS Theory Manual Version 6.9, 2009, ABAQUS Inc.
56. Stewart JR, Gullerud AS, Heinstein MW, Solution verification for explicit transient dynamics problems in the presence of hourglass and contact forces. J Comp Methods App Mech Eng 2006; 195: 1499–1516.

Table 1. Possible combinations for estimating the delamination location using a sequential scan of a transducer network with three transducers for delamination located at different zones

| **Actuator** | Transducer 1 | | Transducer 2 | | Transducer 3 | |
|---|---|---|---|---|---|---|
| **Receiver** | Transducers 2 & 3 | | Transducers 1 & 3 | | Transducers 1 & 2 | |
| Zone 1 | $d_{d\text{-}2} \approx d_{d\text{-}3}$ | $d_{d\text{-}2}$<br>$d_{d\text{-}3} > 0$ | $d_{d\text{-}3} > d_{d\text{-}1}$ | $d_{d\text{-}1}$<br>$d_{d\text{-}3} > 0$ | $d_{d\text{-}2} > d_{d\text{-}1}$ | $d_{d\text{-}1}$<br>$d_{d\text{-}2} > 0$ |
| Zone 2 | $d_{d\text{-}2} \approx 0$ | $d_{d\text{-}3} \approx 0$ | $d_{d\text{-}1} \approx 0$ | $d_{d\text{-}3} > 0$ | $d_{d\text{-}1} \approx 0$ | $d_{d\text{-}2} > 0$ |
| Zone 3 | $d_{d\text{-}2} > 0$ | $d_{d\text{-}3} \approx 0$ | $d_{d\text{-}1} > 0$ | $d_{d\text{-}3} \approx 0$ | $d_{d\text{-}1} \approx 0$ | $d_{d\text{-}2} \approx 0$ |
| Zone 4 | $d_{d\text{-}2} > d_{d\text{-}3}$ | $d_{d\text{-}2}$<br>$d_{d\text{-}3} > 0$ | $d_{d\text{-}1} > d_{d\text{-}3}$ | $d_{d\text{-}1}$<br>$d_{d\text{-}3} > 0$ | $d_{d\text{-}1} \approx d_{d\text{-}2}$ | $d_{d\text{-}1}$<br>$d_{d\text{-}2} > 0$ |

Table 2. Elastic properties of the lamina

| $E_{11}$ (GPa) | $E_{22}$ (GPa) | $E_{33}$ (GPa) | $G_{11}$ (GPa) | $G_{12}$ (GPa) | $G_{13}$ (GPa) | $v_{12}$ | $v_{13}$ | $v_{23}$ |
|---|---|---|---|---|---|---|---|---|
| 120.20 | 7.47 | 7.47 | 3.94 | 3.94 | 2.31 | 0.32 | 0.32 | 0.33 |

Table 3. Summary of delamination sizes and through-thickness locations of damage cases for each scenario in numerical studies

| Delamination length to wavelength ratio (d/λ) | Delamination through-thickness location | | |
|---|---|---|---|
| | 1st and 2nd layer | 2nd and 3rd layer | 3rd and 4th layer |
| d/λ = 0.25 | Case $A_1$ | Case $A_2$ | Case $A_3$ |
| d/λ = 0.50 | Case $B_1$ | Case $B_2$ | Case $B_3$ |
| d/λ = 0.75 | Case $C_1$ | Case $C_2$ | Case $C_3$ |
| d/λ = 1.00 | Case $D_1$ | Case $D_2$ | Case $D_3$ |

Table 4. Summary of all results for Scenario 1 in the numerical case studies

| Damage case | Estimated arrival time | | Estimated delamination location* | True delamination location* |
|---|---|---|---|---|
| | $t_{2f_c}(\mu sec)$ | $t_{f_c}(\mu sec)$ | $d_{d-2}\,(mm)$ | $\bar{d}_{d-2}\,(mm)$ |
| A1 | 98.4 | 65.1 | 23.2 | 23-27 |
| A2 | 99.0 | 65.6 | 23.3 | 23-27 |
| A3 | 96.8 | 64.8 | 23.3 | 23-27 |
| B1 | 100.3 | 66.0 | 23.9 | 21-29 |
| B2 | 100.9 | 63.7 | 25.9 | 21-29 |
| B3 | 100.3 | 66.6 | 23.5 | 21-29 |
| C1 | 100.3 | 66.1 | 23.8 | 19-31 |
| C2 | 101.9 | 66.2 | 24.9 | 19-31 |
| C3 | 103.7 | 67.1 | 25.5 | 19-31 |
| D1 | 102.4 | 65.2 | 25.9 | 17-33 |
| D2 | 100.0 | 65.6 | 24.0 | 17-33 |
| D3 | 99.5 | 65.3 | 23.8 | 17-33 |

* Delamination location from Transducer 2 and between Transducers 2 and 3.

Table 5. Summary of all results for Scenario 2 in the numerical case studies

| Damage case | Estimated arrival time | | Estimated delamination location* | True delamination location* |
|---|---|---|---|---|
| | $t_{2f_c}(\mu sec)$ | $t_{f_c}(\mu sec)$ | $d_{d-3}\ (mm)$ | $\bar{d}_{d-3}\ (mm)$ |
| A1 | 110.5 | 66.6 | 30.8 | 29-33 |
| A2 | 116.1 | 67.3 | 32.5 | 29-33 |
| A3 | 113.1 | 67.4 | 31.8 | 29-33 |
| B1 | 110.0 | 66.7 | 30.2 | 25-33 |
| B2 | 109.6 | 66.3 | 30.3 | 25-33 |
| B3 | 102.1 | 66.3 | 25.7 | 25-33 |
| C1 | 98.7 | 66.4 | 22.5 | 21-33 |
| C2 | 98.7 | 65.8 | 22.9 | 21-33 |
| C3 | 950 | 64.8 | 21.3 | 21-33 |
| D1 | 100.3 | 66.5 | 23.5 | 17-33 |
| D2 | 104.2 | 67.0 | 25.9 | 17-33 |
| D3 | 99.2 | 66.4 | 22.9 | 17-33 |

* Delamination location from Transducer 3 and between Transducer 3 and beam end.

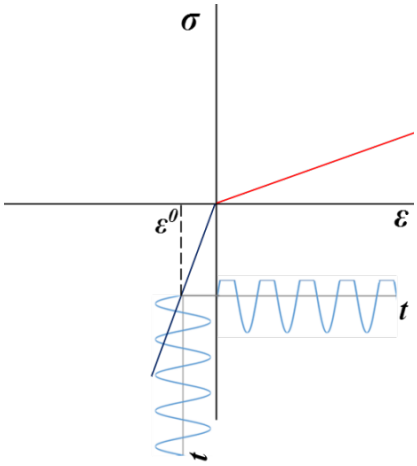


Fig. 1. CAN strain-stress model and wave rectification

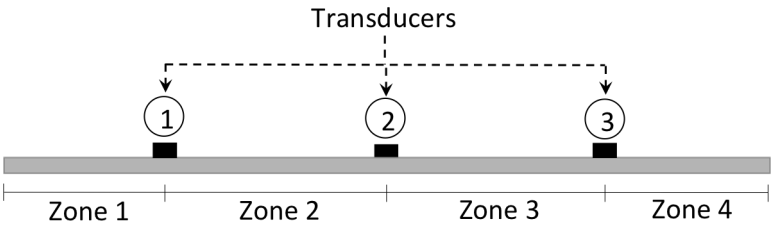


Fig. 2. Schematic diagram of a transducer network for detecting and locating delaminations

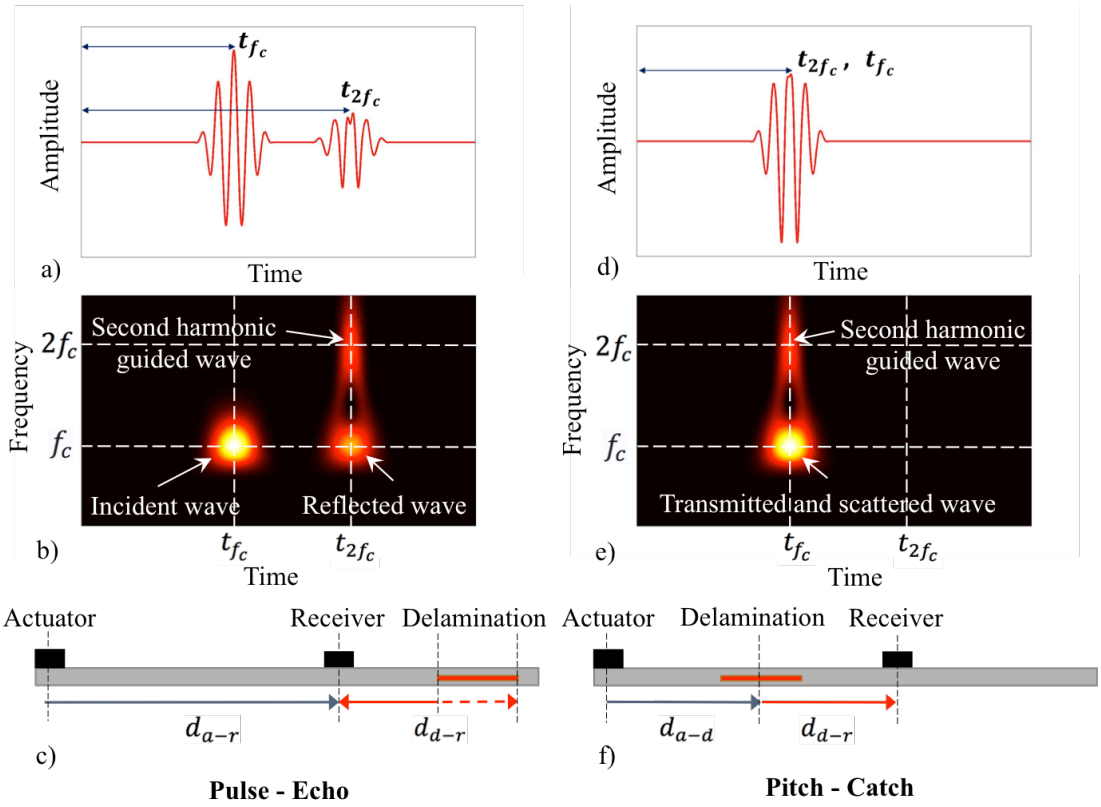


Fig. 3. Typical signal in time domain, time-frequency domain and schematic diagram of the (a)-(c) pulse-echo and (d)-(f) pitch-catch condition

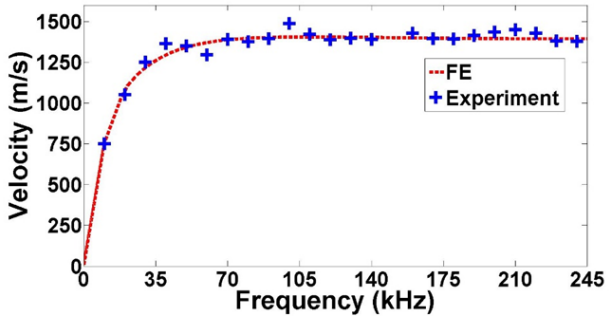


Fig. 4. Group velocity dispersion curves of $A_0$ mode guided wave

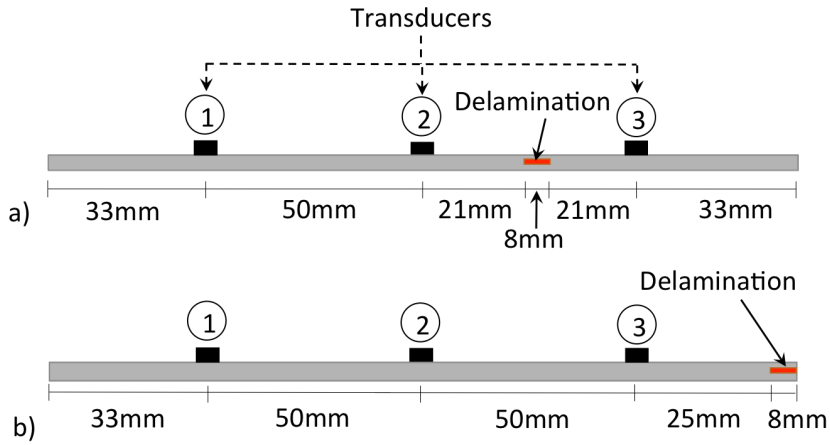


Fig. 5. Schematic diagram of Scenarios a) 1 and b) 2 in numerical case studies

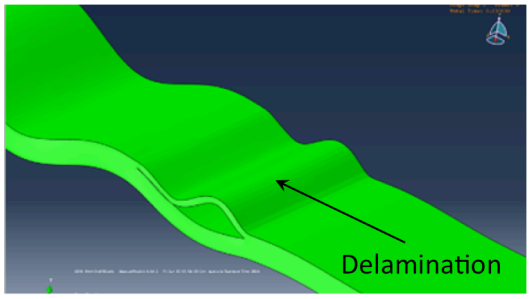


Fig. 6. A snapshot of the $A_0$ guided wave interacting with the delamination in Damage Case $B_3$

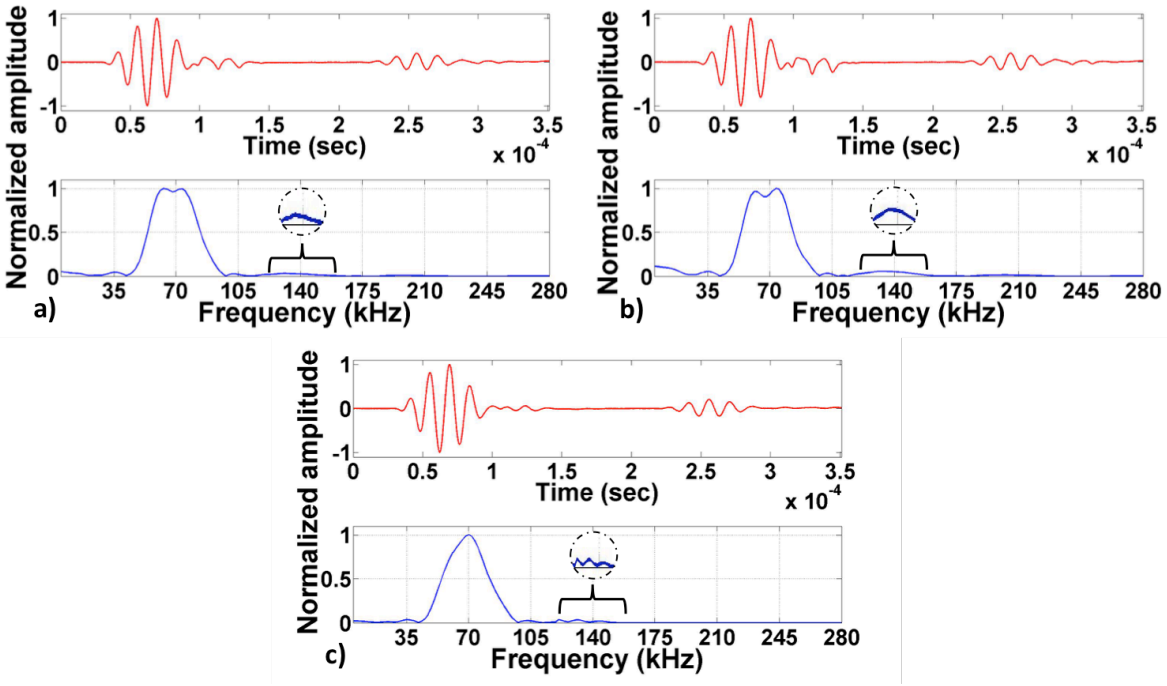


Fig 7. Simulated signal in time-domain and frequency-domain for Damage Cases a) $B_1$ b) $B_2$ and 3) $B_3$ in numerical case studies

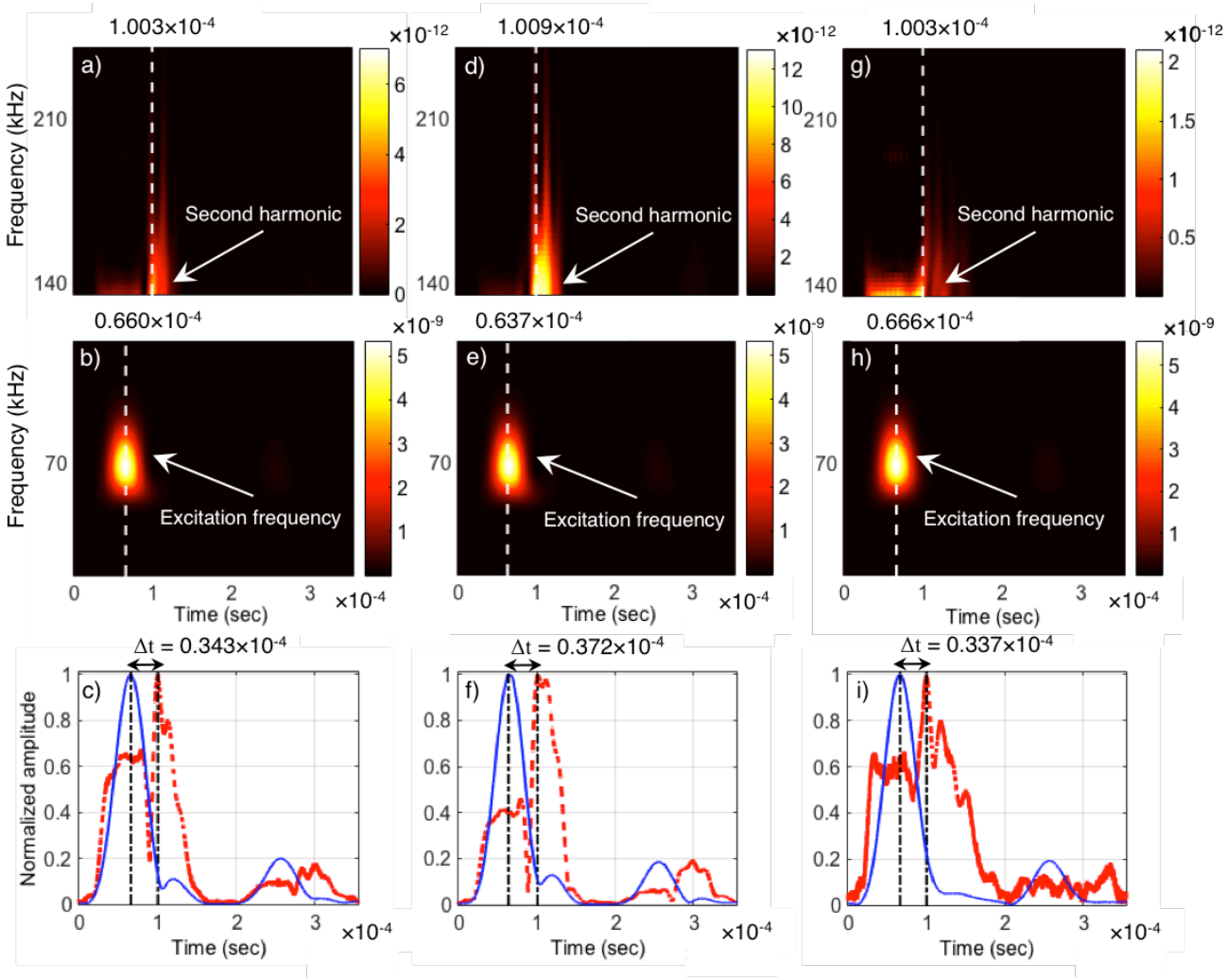


Fig. 8. Time-frequency energy density spectrum, and corresponding normalised wavelet coefficient at excitation frequency (solid line) and second harmonic frequency (dashed line) for Damage Cases (a)-(c) $B_1$, (d)-(f) $B_2$ and (g)-(i) $B_3$ (vertical dash-dotted lines: estimated arrival times)

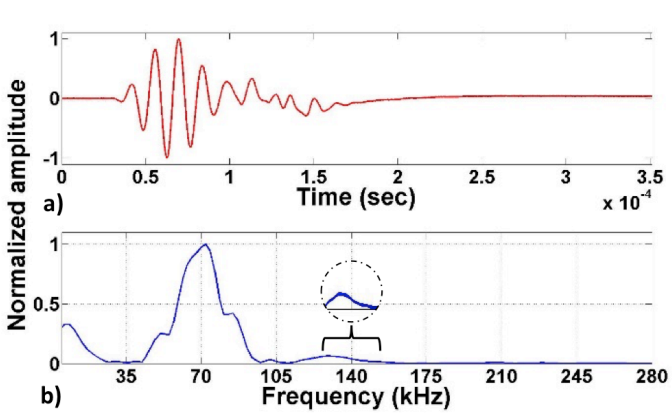


Fig. 9. Simulated signal in time-domain and frequency-domain for Damage Case $C_2$ in numerical case studies

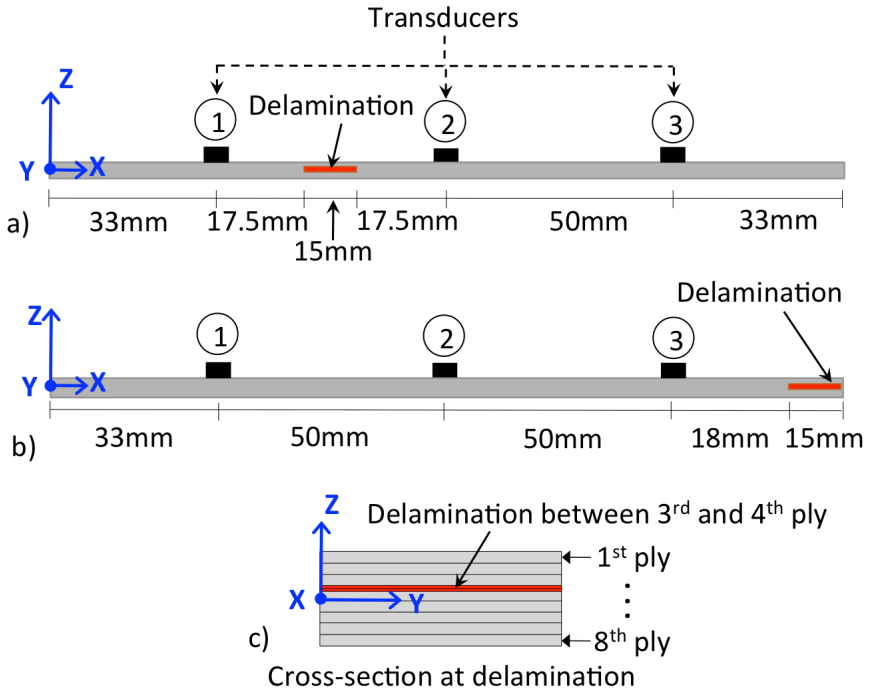


Fig. 10. Schematic diagram of composite beam specimens with a delaminations for a) Damage Case 1 b), Damage Case 2 and c) cross-section at delamination location in experimental case studies

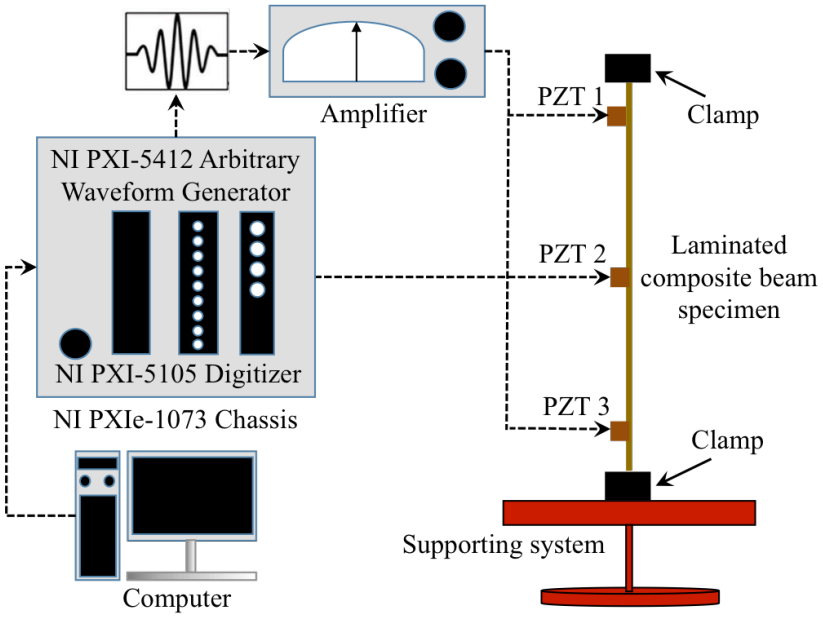


Fig. 11. Experimental setup

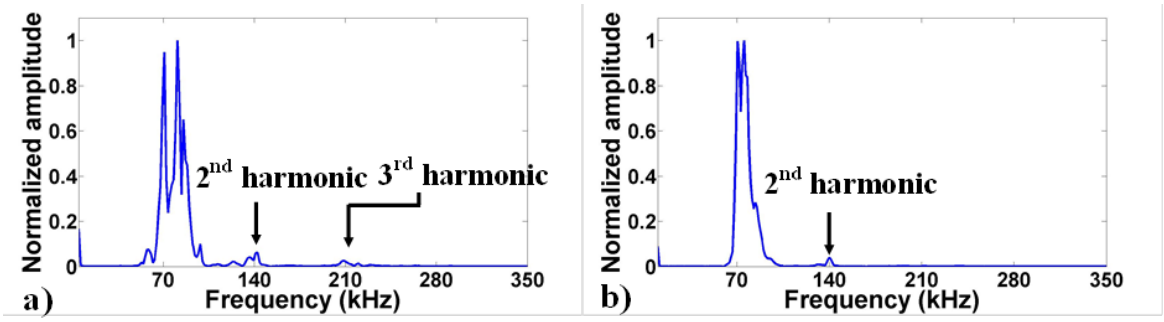


Fig. 12. Measured signal in frequency-domain, a) Transducer 2 is the receiver while Transducer 3 is the actuator in Damage Case 1, b) Transducer 3 is the receiver while Transducer 2 is the actuator in Damage Case 2

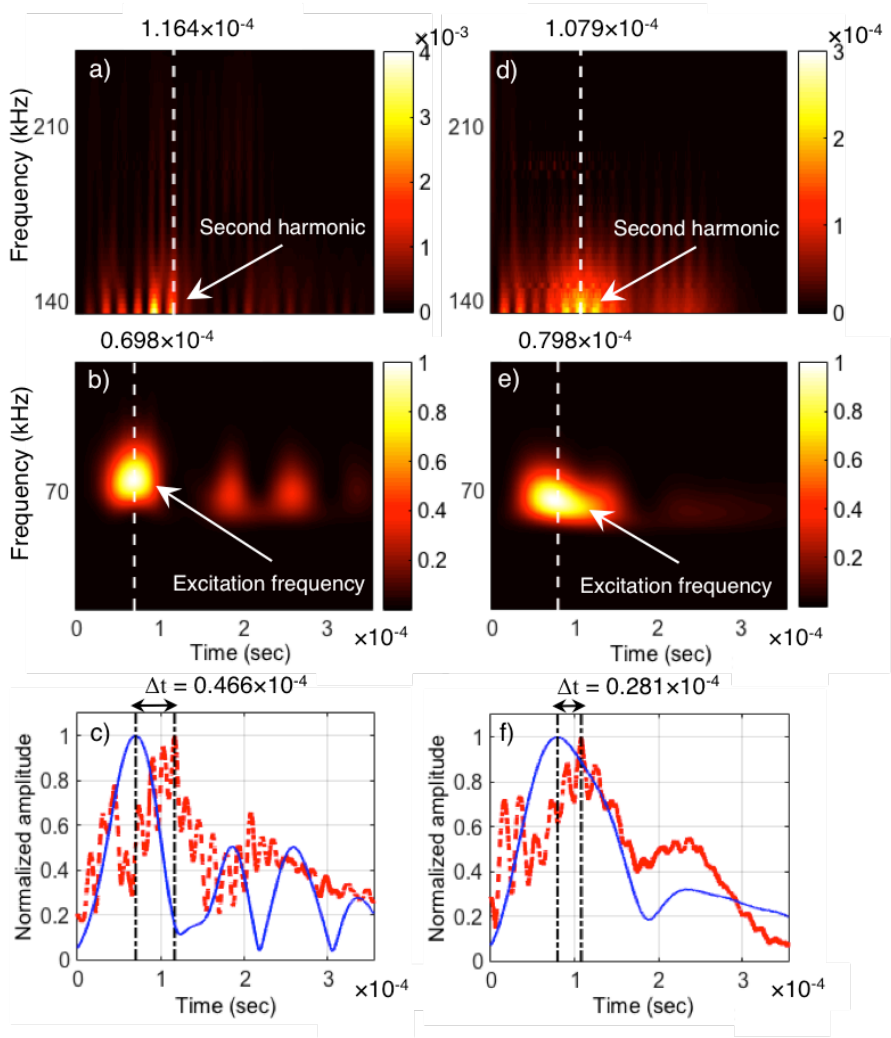


Fig. 13. Time-frequency energy density spectrum zoom-in, and the corresponding normalised CWT coefficients at excitation frequency (solid line) and second harmonic frequency (dashed line) for a) Damage Case 1 and b) Damage Case 2. (vertical dash-dotted lines: estimated arrival times)